Journal of Harbin Engineering University
ISSN: 1006-7043

Vol 47 No.7
July 2026

Numerical Simulation of Thermal Barrier Materials for EV Battery Pack Safety

Le Minh

Vinh Long University of Technology Education, Vinh Long Province, Viet Nam

Abstract

This study develops a computationally efficient framework for screening thermal barrier materials (TBMs) intended to delay thermal propagation (TP) in lithium-ion battery packs for battery electric vehicles (BEVs). A transient one-dimensional heat-conduction model is solved by the implicit finite difference method (IFDM) to predict the temperature evolution through a multilayer TBM-aluminium assembly exposed to a severe jet-fire-like thermal boundary condition. Six TBM concepts, including high- and low-performance intumescent coatings, mica-based laminates, a glass-fiber-reinforced polymer composite with a thermal blanket, a rigid mica-silicone laminate and an ablative material, are represented using effective temperature-dependent thermophysical properties. The novelty of the work is the combination of a stable IFDM formulation, simplified effective-property descriptions of intumescent and ablative mechanisms, and safety-oriented ranking metrics linked to the five-minute evacuation requirement of GB 38031-2020. The results indicate that the 3.5 mm ablative TBM provides the strongest protection, limiting the cold-face peak temperature to 156.7 °C and maintaining a 10.0 min thermal delay. Compared with the worst-performing configurations, this corresponds to an 86.9% reduction in peak cold-face temperature and a 100% positive margin over the GB 38031-2020 delay criterion. The high-performance intumescent coating satisfies the delay requirement marginally, with a 5.1 min delay, whereas thin mica-based and low-performance intumescent solutions fail rapidly. The model is intended as an early-stage design and ranking tool for the VLUTE SMART LI PACK rather than a replacement for full CFD/FEM fire simulations or pack-level abuse tests. Its main limitations are the one-dimensional heat-transfer assumption, the use of effective material properties and the absence of full stochastic validation.

Keywords: Thermal barrier material, thermal propagation, EV battery safety, thermal runaway, implicit finite difference method, uncertainty analysis

1. Introduction

The rapid growth of battery electric vehicles (BEVs) has made lithium-ion battery safety a central issue in automotive engineering. Thermal runaway (TR) and subsequent thermal propagation (TP) between neighbouring cells, modules or structural components remain among the most critical failure modes because a local cell failure can escalate into a pack-level thermal event [1], [2], [8], [10], [15].

Experimental and analytical studies show that large-format Li-ion cells can release heat at the order of tens of kilowatts during TR, accompanied by hot gases, jet flames, molten particles and rapid temperature rise at adjacent components [14], [23], [24]. These mechanisms have motivated extensive research on TR initiation, propagation modelling, fire mitigation, pack architecture and passive thermal-protection materials [1], [2], [8], [10], [15], [24].

Safety standards have therefore introduced explicit propagation-delay requirements. The Chinese national standard GB 38031-2020, for example, requires sufficient warning and evacuation time after a cell-level thermal runaway event in a traction battery system [5]. This regulatory context has accelerated the development of flame-retardant battery pack cases, inter-cell barriers, module-level insulation and other passive measures that delay heat transfer from the failed cell or module to the surrounding pack structure [5], [6], [20], [21].

Among passive measures, thermal barrier materials (TBMs) are particularly attractive because they can be placed between cells, between modules, or between the module and the pack enclosure without increasing the complexity of active cooling control. Seshadri et al. evaluated representative TBMs for battery electric vehicles, including intumescent coatings, ablative layers, mica-based laminates and composite barriers under jet-fire-like exposure, and showed that energy-absorbing mechanisms such as endothermic decomposition and char formation strongly affect thermal delay [7].

However, full-scale pack tests and high-fidelity numerical simulations remain expensive and time-consuming when the design space includes material type, thickness, density, placement and enclosure geometry. Recent CFD and finite-element studies can resolve gas-phase combustion, venting and three-dimensional heat transfer, but they often require detailed geometry, calibrated source terms and substantial computational resources [6], [25]. Conversely, reduced-order and one-dimensional models are faster, but they must be positioned carefully with respect to their assumptions and uncertainty [26], [27].

The research gap addressed in this paper is the lack of a transparent, low-cost numerical screening framework that can compare practical TBM concepts under a common severe thermal load while retaining the dominant heat-storage and insulation mechanisms of ablative and intumescent materials. The proposed model is not intended to replace detailed CFD/FEM validation. Instead, it provides a first-pass ranking method that can identify promising TBM candidates before more expensive module- or pack-level tests are performed. The main contributions are as follows:

- (i) A numerically stable one-dimensional transient heat-conduction framework for multilayer EV battery-pack walls, solved using the implicit finite difference method (IFDM).

- (ii) An effective material-modelling strategy that represents ablative heat absorption and intumescent char insulation through temperature-dependent specific heat, thermal conductivity and density.

- (iii) A comparative performance evaluation of six TBM configurations using peak cold-face temperature, delay to critical temperature and compliance with the GB 38031-2020-inspired five-minute safety criterion.

Table 1 summarizes how the present IFDM screening model differs from recent CFD, finite-element, reduced-order and passive-barrier modelling approaches. The comparison clarifies the intended role of the model: rapid TBM ranking for early design, with explicit recognition that gas venting, radiation, three-dimensional pack geometry and stochastic propagation behavior require higher-fidelity follow-up analysis.

The scope of the present model is therefore deliberately narrow: it evaluates conductive heat penetration through candidate TBM/enclosure stacks under a common severe boundary condition. This limitation is explicitly considered when interpreting the results and motivates the future extension to 2D/3D geometries and pack-level validation.

Table 1. Comparison of numerical approaches for thermal runaway/thermal propagation and passive thermal-barrier assessment in EV battery packs.

Approach	Typical use	Main limitations	Role in this work
CFD/FEM models [6], [25]	3D gas/fire dynamics, venting and pack-case heat transfer	High mesh/data cost; detailed geometry and source terms required	Follow-up validation path for selected TBMs
Reduced-order or lumped models [27]	Fast pack-level thermal runaway propagation and uncertainty studies	Limited spatial resolution; calibrated lumped parameters required	Related screening philosophy; present model retains through-thickness gradients
PCM/passive BTMS	Latent-heat buffering and hybrid cooling in	Usually target operating-	Complementary thermal

models [9], [28]	normal operation	temperature control, not direct jet-fire barriers	management strategy
TBM jet-fire experiments [7]	Direct material/system evidence under severe fire exposure	Costly and limited to tested material-thickness combinations	Material basis and qualitative ranking benchmark
Present IFDM TBM model	1D multilayer TBM/enclosure conduction with effective ablative/intumescent properties	No gas-phase combustion, radiation coupling, lateral spreading or full stochastic validation	Early-stage ranking tool for VLUTE SMART LI PACK

2. Mathematical model and numerical method

2.1. Governing equations and numerical discretization

A one-dimensional transient heat-conduction model with temperature-dependent effective properties and, where applicable, an internal endothermic heat sink is used to describe heat transport through the multilayer TBM assembly. The governing partial differential equation is given by

$$\rho(T)C_p(T)\frac{\partial T(x,t)}{\partial t}=\frac{\partial}{\partial x}\left[k(T)\frac{\partial T(x,t)}{\partial x}\right]+\dot{q}_{chem'''}(x,t) \quad (1)$$

where ρ is density (kg/m³), Cp is specific heat capacity (J/kg.K), k is thermal conductivity (W/m.K), and q_{sink} denotes the volumetric heat sink associated with pyrolysis, phase change or other endothermic processes within the TBM layer (W/m³).

Thermal degradation of ablative materials is modeled by a first-order Arrhenius-type reaction. The evolution of the degree of conversion is described by:

$$\frac{d\alpha}{dt}=A\exp\left(-\frac{E_a}{RT}\right)(1-\alpha) \quad (2)$$

where A is the pre-exponential factor (s⁻¹), E_a is the activation energy (J/mol), and R is the universal gas constant (8.314 J/mol.K). The associated endothermic heat sink is:

$$\dot{q}_{chem'''}=-\rho_0\Delta H_{pyr}\frac{d\alpha}{dt} \quad (3)$$

To retain computational efficiency while capturing endothermic behaviour, the chemical sink is represented through an effective specific heat capacity over the active decomposition interval:

$$C_{p,eff}(T)=C_p(T)+\frac{\eta\Delta H_{pyr}}{T_{end}-T_{onset}} \quad \text{for} \quad T_{onset}\le T\le T_{end} \quad (4)$$

where η is the reaction-efficiency factor calibrated from thermogravimetric analysis (TGA). The thermal conductivity and density are then updated piecewise as functions of the degree of conversion:

$$k(T)=k_v+(k_c-k_v)\alpha \quad (5)$$

$$\rho(T)=\rho_v-(\rho_v-\rho_c)\alpha \quad (6)$$

The hot face (x = 0) is subjected to a time-dependent jet-fire temperature profile:

$$T(0,t)=T_{jet}(t)=T_\infty+(T_{max}-T_\infty)\left[1-\exp\left(-\frac{t}{\tau}\right)\right] \quad (7)$$

where a and b control the ramp rate. The cold face (x = L) exchanges heat with ambient air through convection, represented by the Robin boundary condition:

$$-k\frac{\partial T}{\partial x}\Big|_{x=L}=h_c\left[T(L,t)-T_\infty\right] \quad (8)$$

with h_c denoting the convective heat-transfer coefficient. The initial condition assumes a uniform ambient temperature:

$$T(x,0)=T_0=25^{\circ}\text{C} \quad (9)$$

The spatial domain is discretized into N nodes with uniform spacing Δx, and the temperature field is advanced with a time step Δt. Using a fully implicit strategy for Eq. (1) gives the following expression for an interior node at time level n+1:

$$-\lambda_j T_{j-1}^{n+1} + \left(1 + 2\lambda_j\right) T_j^{n+1} - \lambda_j T_{j+1}^{n+1} = T_j^n \quad (10)$$

where Fo is the local Fourier number evaluated at the new time level. The resulting system of algebraic equations at each time step has a tridiagonal form:

$$\mathbf{A}\mathbf{T}^{n+1} = \mathbf{b} \quad (11)$$

with the coefficient matrix, solution vector, and right-hand side vector given by:

$$\mathbf{A} = \begin{bmatrix} 1 & 0 & \cdots & 0 \\ -\lambda_2 & 1+2\lambda_2 & -\lambda_2 & 0 \\ 0 & -\lambda_3 & 1+2\lambda_3 & -\lambda_3 \\ \vdots & \ddots & \ddots & \vdots \\ 0 & \cdots & -\lambda_{N-1} & 1+2\lambda_{N-1} \\ 0 & \cdots & 0 & 1 \end{bmatrix} \quad (12)$$

The tridiagonal matrix is solved using the Thomas algorithm (TDMA). The implicit formulation is unconditionally stable for linear conduction and is well suited to the steep temperature gradients near the hot face during jet-fire exposure [10], [11].

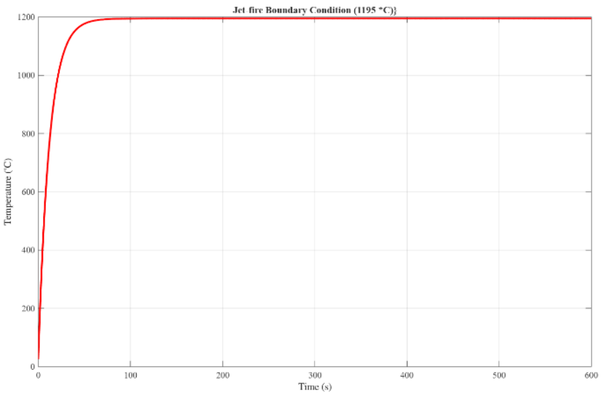

Figure 1. Jet-fire boundary condition applied at the hot face of the multilayer TBM assembly: temperature ramps from ambient to 1195 °C within approximately 40 s and is then maintained to represent severe thermal exposure for EV battery-pack safety screening.

The thermal boundary condition applied at the hot face (x = 0) is illustrated in Figure 1. This profile represents a severe jet-fire exposure scenario commonly encountered during thermal runaway events in EV battery packs. The temperature rapidly increases from ambient conditions (25 °C) to a peak of 1195 °C within approximately 40 seconds, simulating the intense heat flux generated by burning electrolyte and adjacent cell failures. After reaching the peak, the temperature is maintained constant for the remaining 600 seconds of the simulation duration.

This boundary condition is consistent with experimental jet-fire testing protocols used for evaluating thermal barrier materials in battery electric vehicles [1], [7]. The rapid ramp rate (approximately 30 °C/s) and sustained high temperature create extreme thermal gradients across the TBM layers, providing a rigorous test of the material's ability to protect the aluminium backing and prevent thermal propagation to neighbouring cells. The selected profile aligns with the safety requirements outlined in GB 38031-2020, which mandates sufficient thermal protection to allow occupant evacuation within 5 minutes of thermal runaway initiation [5].

2.2. Material configurations and simulation setup

Six TBM configurations are considered based on the experimental matrix reported for battery electric vehicle passive fire protection [7]. Each configuration contains a TBM layer on the hot side and an aluminium backing on the cold side representing the pack case or structural support.

Mat A – High-performance intumescent coating: expands to form a relatively thick char layer (~15 mm) under heat exposure. It is represented using temperature-dependent conductivity and an increased effective heat capacity in the activation range.

Mat B – Low-performance intumescent coating: forms only a thin char layer (~5 mm), with limited expansion and weaker insulation. Its effective thermal conductivity is higher than that of Mat A.

Mat C – Thin mica-ceramic layer (~2 mm): an inorganic electrical insulator with good dielectric strength, but limited heat-storage capacity and insufficient thickness for severe jet-fire exposure.

Mat D – Glass-fiber-reinforced polymer (GFRP) with thermal blanket: a fibre-based composite layer that provides structural support and insulation, but has limited endothermic heat absorption.

Mat E – Ablative material with strong endothermic behaviour: designed to absorb heat through pyrolysis and ablation, producing char and gas release while increasing the effective heat capacity over the active decomposition range.

Mat F – Rigid mica with silicone reinforcement: a mica laminate with silicone binder that improves mechanical integrity and heat resistance, but provides limited thermal delay under direct jet-fire exposure.

For demonstration purposes, the selected materials represent the main TBM classes used in EV battery packs: intumescent coatings, ablative composites, ceramic/mica-based insulators and silicone-based flame-retardant laminates [7], [12], [13]. Performance is evaluated using three metrics: peak cold-face temperature, time to reach critical temperature thresholds (250 °C and 300 °C), and the TBM-aluminium interface temperature gradient, which indicates the ability of the barrier to localize the thermal load.

The simulation workflow used for all TBM cases is summarized in Figure 2. A common thermal boundary condition and identical post-processing metrics are used to ensure that the comparison reflects material and thickness effects rather than changes in numerical setup.

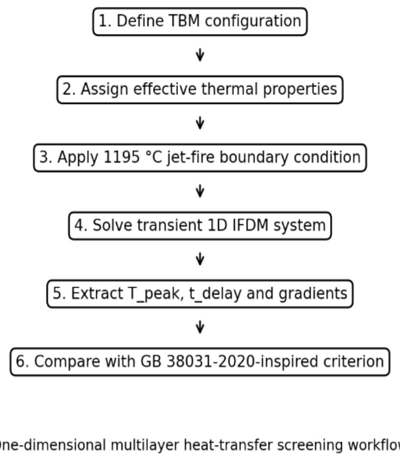

Figure 2. Numerical simulation workflow for TBM screening, from material-configuration definition and effective-property assignment to IFDM solution, metric extraction and GB 38031-2020-inspired safety assessment.

3. Results and discussion

3.1. Cold-face temperature evolution

The simulated cold-face temperature histories separate clearly into two performance groups when evaluated by peak temperature, delay time and compliance with the GB 38031-2020-inspired five-minute criterion.

High-performance TBMs (PASS group). Mat E (ablative) and Mat A (high-performance intumescent) provide meaningful thermal protection relative to the other configurations. Mat E achieves the lowest cold-face peak temperature, 156.7 °C, and remains below the 250 °C threshold during the entire 600 s exposure. Mat A reaches a higher peak temperature of 588.7 °C but still provides a 5.1 min delay before reaching the critical threshold, which is just above the five-minute safety target.

Low-performance TBMs (FAIL group). Mat B (low-performance intumescent), Mat C (thin mica-ceramic), Mat D (GFRP + thermal mat) and Mat F (rigid mica-silicone) fail rapidly under the same boundary condition. Their peak cold-face temperatures approach the imposed hot-face temperature, and their delay times remain below 0.5 min. These results indicate that passive barriers relying only on small thickness or nominally low conductivity, without sufficient endothermic heat absorption or char expansion, are not adequate as primary protection layers under severe jet-fire exposure.

The numerical ranking is consistent with the qualitative trend reported in jet-fire-like TBM experiments, where ablative materials and high-performance intumescent coatings outperformed thin mica-based and low-performance intumescent barriers [7].

The numerical results illustrating the cold-face temperature evolution are presented in Figure 3. The thermal response of the evaluated TBMs diverges into two distinct performance categories based on their ability to delay heat transfer.

High-performance TBMs: The ablative material (Mat E) maintains the cold-face temperature below the 250 °C threshold throughout the 600 s exposure, reaching a peak value of only 156.7 °C. The high-performance intumescent coating (Mat A) reaches a higher peak temperature but delays threshold crossing to 5.1 min, narrowly satisfying the safety criterion. These trends confirm that endothermic decomposition and char formation are more effective than simple low-conductivity insulation under the imposed boundary condition.

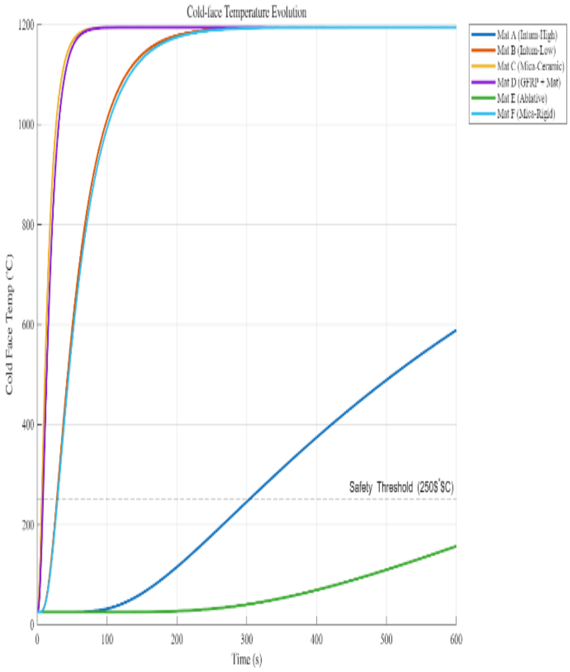

Figure 3. Simulated cold-face temperature evolution of the six TBM configurations under a 1195 °C jet-fire boundary condition. The dashed line indicates the 250 °C safety threshold used for delay-time assessment, and the curves show the clear separation between energy-absorbing TBMs and rapidly failing thin barriers.

Low-performance TBMs: In contrast, Mat B, Mat C, Mat D and Mat F exhibit rapid thermal failure. Their cold-face temperatures approach the hot-face temperature, and their delay times are below 0.5 min. The result indicates that thin mica layers, low-expansion intumescents and structural fiber layers should not be selected as standalone primary barriers for severe jet-fire exposure.

Table 2. Summary of numerical simulation results and safety compliance for the evaluated TBMs. The delay criterion is interpreted against the five-minute requirement of GB 38031-2020.

TBM configuration	**Peak cold-face temperature T_peak (°C)**	**Thermal delay t_delay (min)**	**Safety status (GB 38031-2020)**
Mat A (Intum-High)	588.7	5.1	PASS
Mat B (Intum-Low)	1194.4	0.5	FAIL
Mat C (Mica-Ceramic)	1194.7	0.1	FAIL
Mat D (GFRP + Mat)	1194.7	0.1	FAIL
Mat E (Ablative)	156.7	10.0	PASS
Mat F (Mica-Rigid)	1194.6	0.5	FAIL

Table 3. Quantitative improvement metrics relative to the worst-case cold-face peak temperature (1194.7 °C) and the five-minute GB 38031-2020-inspired delay requirement.

TBM configuration	**Peak-temperature reduction vs. worst case (%)**	**Delay margin vs. 5 min criterion (%)**	**Interpretation**
Mat A (Intum-High)	50.7	+2.0	PASS but marginal delay margin

Mat B (Intum-Low)	0.0	-90.0	FAIL; minimal peak reduction
Mat C (Mica-Ceramic)	0.0	-98.0	FAIL; reference worst case
Mat D (GFRP + Mat)	0.0	-98.0	FAIL; reference worst case
Mat E (Ablative)	86.9	+100.0	PASS with robust safety margin
Mat F (Mica-Rigid)	0.0	-90.0	FAIL; minimal delay margin

The percentage metrics clarify the practical significance of the ranking. Mat E reduces the peak cold-face temperature by 86.9% relative to the worst-case barrier and doubles the required delay time. Mat A reduces the peak temperature by 50.7%, but its +2.0% delay margin is small; therefore, its pass status should be treated as sensitive to material-property scatter, local thickness variation and boundary-condition uncertainty. The failure group has negligible peak-temperature reduction and a delay deficit of 90–98%, making their ranking insensitive to ordinary numerical or property perturbations.

Recent uncertainty-aware TRP models show that variations in thermal conductivity, specific heat, reaction kinetics and latent heat can strongly affect predicted propagation timing [26], [27]. For this reason, the present deterministic screening model should be interpreted through safety margins rather than only through pass/fail labels. The large separation between Mat E and the failure group supports a robust first-place ranking, whereas the small margin of Mat A indicates that follow-up CFD/FEM or experimental validation is necessary before final pack design. A full Monte Carlo uncertainty analysis is therefore recommended for future work once calibrated material-property distributions become available.

The thermal protection delay capabilities of the evaluated TBMs are summarized in Figure 4, highlighting their compliance with the GB 38031-2020-inspired criterion, which requires a minimum 5-minute evacuation window during a thermal event.

Mat E (Ablative) demonstrates exceptional performance, providing a thermal delay of 10.0 minutes, which is double the regulatory requirement. This significant safety margin suggests that ablative materials not only prevent immediate structural failure but also allow ample time for active safety systems (such as fire suppression) to engage or for passengers to evacuate safely.

Mat A (High-performance Intumescent) achieves a delay of 5.1 minutes, barely meeting the safety threshold. While technically compliant, its marginal performance implies that any variation in material thickness or heat flux intensity could compromise its effectiveness.

Conversely, the remaining configurations (Mat B, Mat C, Mat D, and Mat F) exhibit negligible thermal delays ranging from 0.1 to 0.5 minutes. These materials fail to provide the necessary time buffer, confirming their unsuitability as primary thermal barriers for high-safety EV battery packs.

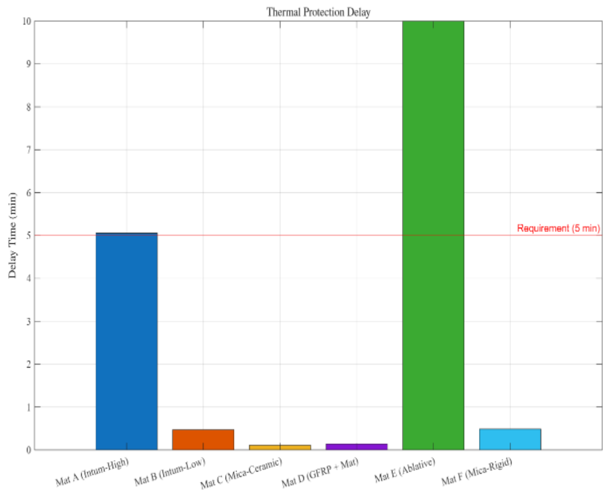

Figure 4. Thermal protection delay of the six TBM configurations compared with the five-minute GB 38031-2020-inspired evacuation requirement. Mat E provides the largest margin, whereas Mat A only marginally satisfies the delay criterion.

3.2. Temperature distribution and thermal gradients

Although the governing model is one-dimensional, the through-thickness temperature histories are visualized as time-dependent profiles and heatmaps to clarify the barrier mechanism. For Mat E, a steep temperature gradient forms near the hot face and the TBM-aluminium interface remains comparatively cool, indicating that the ablative layer confines most of the thermal load to the exposed side. This behavior is consistent with strong endothermic heat absorption and reduced effective diffusivity during degradation.

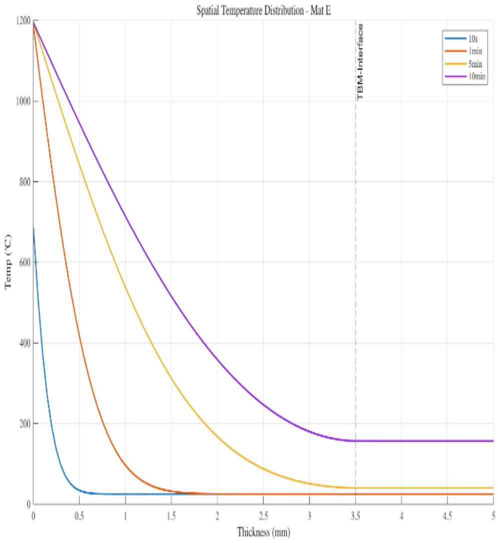

Figure 5. Spatial temperature distribution through the thickness of Mat E (ablative) at selected times (10 s, 1 min, 5 min and 10 min). The dashed vertical line marks the TBM-Aluminium interface at x = 3.5 mm, highlighting the thermal cut-off region formed near the hot face.

To visualize the heat transfer mechanism through the thickness, Figure 5 presents the temperature field evolution. For Mat E (Figure 5a), a pronounced thermal cutoff zone is established near the hot face, characterized by a steep temperature gradient that confines high temperatures to the exposed side. This confirms the effectiveness of the ablative mechanism in dissipating energy before it reaches the aluminium backing. Conversely, Mat C (Figure 5b) exhibits a smooth, nearly linear temperature gradient, indicating rapid conductive heat transfer with minimal thermal resistance. This uniform penetration correlates directly with the high cold-face temperatures observed in Figure 4, validating the model's capability to distinguish between conductive and absorptive thermal behaviours.

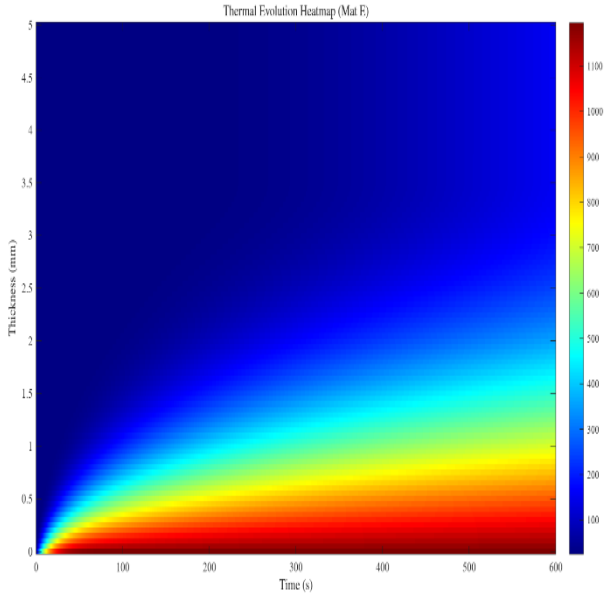

Figure 6. Spatial-temporal temperature distribution through the thickness of Mat E during the 600 s jet-fire exposure. The heatmap illustrates the restricted heat-penetration front and the effective separation of the cold face from the external fire environment.

The spatial-temporal thermal evolution of Mat E is visualized in Figure 6. The heatmap shows a restricted thermal penetration front: despite the severe jet-fire boundary condition at the hot face (x = 0 mm), the high-temperature zone (>600 °C) remains confined close to the exposed surface during most of the 600 s simulation. At the end of exposure, the thermal wave has not penetrated deeply enough to raise the cold face above the critical threshold, which corroborates the peak cold-face temperature of 156.7 °C reported in Table 2.

The quantitative margins reinforce the visual interpretation of Figures 5 and 6. Mat E maintains the cold-face temperature below 200 °C during the full exposure, while Mat A provides a useful but less robust delay. The remaining configurations reach critical temperatures too quickly to act as standalone thermal barriers under severe jet-fire exposure.

3.3. Design implications for VLUTE SMART LI PACK

The numerical results provide the following design implications for the VLUTE SMART LI PACK:

(i) Ablative TBMs provide the best thermal protection-to-thickness ratio in the simulated configuration, achieving 10.0 min of delay with only a 3.5 mm layer.

(ii) High-performance intumescent coatings can satisfy the minimum delay criterion when sufficient char expansion is achieved, but the marginal +2.0% delay margin suggests that manufacturing tolerance and ageing must be evaluated carefully.

(iii) Thin mica-based and low-performance intumescent layers should not be used as the primary barrier under severe jet-fire exposure; their role should be limited to dielectric insulation, spacing control or secondary protection when combined with an energy-absorbing TBM.

Overall, a multifunctional enclosure combining an ablative or high-performance intumescent TBM with structural and electrical-insulation layers is the most promising strategy for safer and lighter EV battery packs under contemporary safety standards such as GB 38031-2020 [5], [6].

4. Conclusions

This work presents a computational framework for evaluating TBMs in EV battery packs using a one-dimensional transient heat-conduction model solved with an implicit finite difference method. The framework provides a fast screening tool for material ranking under severe jet-fire-like exposure. The main conclusions are as follows:

(i) The IFDM formulation is stable for the steep temperature gradients generated by the 1195 °C hot-face boundary condition and is suitable for rapid comparison of multilayer TBM/enclosure stacks.

(ii) The ablative TBM is the best-performing configuration. For a 3.5 mm layer, it limits the cold-face peak temperature to 156.7 °C, corresponding to an 86.9% reduction relative to the worst-case TBM response, and provides a 10.0 min thermal delay, which is 100% above the GB 38031-2020-inspired five-minute criterion.

(iii) The high-performance intumescent coating provides a secondary protection option, reducing peak cold-face temperature by 50.7% relative to the worst case and meeting the delay requirement with 5.1 min. Because this margin is only +2.0%, it should be validated under realistic property scatter, ageing and manufacturing tolerances before final adoption.

(iv) Low-performance intumescent, thin mica-ceramic, GFRP/thermal-mat and rigid mica-silicone configurations fail to provide sufficient delay under the imposed boundary condition. Their 90–98% delay deficits indicate that they should be treated as auxiliary electrical or structural layers rather than standalone thermal-propagation barriers.

(v) The principal limitations of the present model are the one-dimensional conduction assumption, the use of effective material properties for complex ablative/intumescent mechanisms, and the absence of full stochastic validation. Future work will extend the model to 2D/3D geometries, couple it with cell-level TR and vent-gas dynamics, and validate the predictions with module- and pack-level experiments [25]–[27].

Nomenclature

t time, [s]

T temperature, [°C] or [K]

x spatial coordinate, [m]

ρ density, [kg/m³]

C_p specific heat capacity, [J/(kg.K)]

k thermal conductivity, [W/(m.K)]

α degree of conversion, [-]

A pre-exponential factor, [s^{-1}]

E_a activation energy, [J/mol]

R universal gas constant, 8.314 [J/(mol.K)]

h_c convective heat transfer coefficient, [W/(m².K)]

L total thickness, [m]

References

[1] Feng, X., Ouyang, M., Liu, X., Lu, L., Xia, Y., He, X. Thermal runaway mechanism of lithium ion battery for electric vehicles: A review. Energy Storage Mater. 10, 246-267 (2018) DOI: 10.1016/j.ensm.2017.10.013

[2] Wang, Q., Mao, B., Stoliarov, S. I., Sun, J. A review of lithium ion battery failure mechanisms and fire prevention strategies. Prog. Energy Combust. Sci.

73, 95-131 (2019) DOI: 10.1016/j.pecs.2019.03.002

[3] Bandhauer, T. M., Garimella, S., Fuller, T. F. A critical review of thermal issues in lithium-ion batteries. J. Electrochem. Soc. 158, R1-R25 (2011) DOI: 10.1149/1.3515880

[4] Spotnitz, R., Franklin, J. Abuse behavior of high-power, lithium-ion cells. J. Power Sources 113, 81-100 (2003) DOI: 10.1016/S0378-7753(02)00488-3

[5] GB 38031-2020. Electric vehicles traction battery safety requirements. Standardization Administration of the People's Republic of China (2020) Beijing

[6] Kim, H. S., Cho, M., Lee, D., Lee, C., Kim, J., Kang, S. Flame-retardant battery pack case design for delaying thermal runaway: A CFD and experimental study. Materials 18(24), 5605 (2025). DOI: 10.3390/ma18245605

[7] Seshadri, N., Cross, D., Fotouhi, A. Experimental evaluation of thermal barrier materials used in battery electric vehicles. Automotive Innovation 9(2) (2026). DOI: 10.1007/s42154-024-00349-1

[8] Liu, P., Liu, C., Liu, K., Zhang, H., Zhao, Y. Thermal runaway and propagation of lithium-ion batteries: A review from cell to pack. J. Energy Storage 44, 103361 (2021) DOI: 10.1016/j.est.2021.103361

[9] Zhang, S., Rao, Z., Xu, X., Li, Y. A review of phase change materials for thermal management of lithium-ion batteries. Renew. Sustain. Energy Rev. 168, 112891 (2022) DOI: 10.1016/j.rser.2022.112891

[10] Ren, D., Liu, X., Lu, L., Ouyang, M., Feng, X. Thermal runaway propagation mechanisms and suppression strategies for lithium-ion battery packs: A review. J. Energy Storage 57, 106643 (2023) DOI: 10.1016/j.est.2022.106643

[11] Pesaran, A. A. Battery thermal models for hybrid vehicle simulations. J. Power Sources 110, 377-386 (2002) DOI: 10.1016/S0378-7753(02)00200-8

[12] Kim, Y., Park, J., Lee, S., Kim, H.: Thermal characterization and fire resistance of intumescent coatings for electric vehicle battery applications. Fire Saf. J. 129, 103512 (2022) DOI: 10.1016/j.firesaf.2021.103512

[13] Chen, M., Zhao, Y., Li, W., Wang, J. Numerical modeling of thermal runaway propagation in battery packs with phase change materials. J. Power Sources 506, 230456 (2021) DOI: 10.1016/j.jpowsour.2021.230456

[14] Wang, S., Zhang, Q., Liu, X., Li, J., Wang, L. Thermal runaway features of large format prismatic lithium-ion batteries using extended volume accelerating rate calorimetry. J. Power Sources 298, 1-10 (2015) DOI: 10.1016/j.jpowsour.2015.08.012

[15] Sun, J., Li, Y., Zhou, T., Yang, K., Zheng, S., Yang, X., Zhou, L., Xiong, R. Modeling of thermal runaway propagation in battery packs: A review. Energy Storage Mater. 44, 384-405 (2022). DOI: 10.1016/j.ensm.2021.10.030

[16] IEC 62660-2:2018. Secondary lithium-ion cells for the propulsion of electric road vehicles – Part 2: Reliability and abuse testing. International Electrotechnical Commission (2018) Geneva

[17] Willstrand, N., Böhmler, W., Temple, A. Safety aspects of large battery packs in electric vehicles. VTI Rapport 797A, Swedish National Road and Transport Research Institute (2014), Linköping

[18] Liu, B., Jia, Y., Li, J., Yin, S., Yuan, C., Xu, J. Safety issues caused by the cell design of lithium ion batteries. J. Mater. Chem. A 6, 21475-21484 (2018) DOI: 10.1039/C8TA08997C

[19] Zhang, G., Li, Z., Sun, Y. Fire hazards of lithium-ion batteries in electric vehicles: A comprehensive review. J. Energy Storage 44, 103361 (2021) DOI: 10.1016/j.est.2021.103361

[20] SAE J2464:2021. Electric and hybrid electric vehicle rechargeable energy storage system (RESS) safety and abuse testing. SAE International (2021) Warrendale

[21] UL 2580. Standard for batteries used in electric vehicles. Underwriters Laboratories Inc. (2021) Northbrook

[22] ISO 6469-3:2018. Electrically propelled road vehicles —safety specifications – Part 3:

Protection of persons against electric shocks. International Organization for Standardization (2018) Geneva

[23] Liu, J., Cheng, Y., Rao, R., Wang, S., Liu, P. Experimental investigation on thermal runaway propagation of large-format lithium-ion batteries with different cathode materials. Appl. Therm. Eng. 219, 119611 (2023) DOI: 10.1016/j.applthermaleng.2022.119611

[24] Feng, X., Zheng, S., He, X., Wang, L., Ren, Y., Ouyang, M., Ren, D. Time sequence analysis of thermal runaway in lithium-ion batteries based on internal short circuit. J. Power Sources 450, 227744 (2020) DOI: 10.1016/j.jpowsour.2020.227744

[25] Wang, B., Kannan, P., Liao, Y.-T., Kwon, B., Premnath, V., Jeevarajan, J. A numerical model for simulating thermal runaway propagation between lithium-ion battery cells with detailed heat transfer analysis. Int. J. Heat Mass Transfer 256, 128073 (2026). DOI: 10.1016/j.ijheatmasstransfer.2025.128073

[26] Kitagawa, H., Takagishi, Y., Nishiuchi, M., Saeki, K., Baba, R., Yamaue, T. Modelling of thermal runaway propagation in Li-ion battery cells considering variations in thermal property measurements. Batteries 11(10), 386 (2025). DOI: 10.3390/batteries11100386

[27] Bugryniec, P. J., Brown, S. F. Lithium-ion battery thermal runaway propagation prevention — predicting critical parameters considering uncertainty. J. Energy Storage 143, 119679 (2026). DOI: 10.1016/j.est.2025.119679

[28] Pal, R. K., Paw, J. K. S., Ganesan, P., Tong, C. W. Modeling and simulation of phase change material-based passive and hybrid thermal management systems for lithium-ion batteries: A comprehensive review. J. Energy Storage (2025). DOI: 10.1016/j.est.2025.116011

[29] Akkuş, F., Işık, M. Z. A review of thermal management systems of lithium-ion batteries used in electric vehicles. J. Traffic Transp. Eng. (Engl. Ed.) (2025). DOI: 10.1016/j.jtte.2025.06.002